Published in final edited form as:
Dent Mater. 2010 November ; 26(11): 1077–1089. doi:10.1016/j.dental.2010.07.008.

A Chemical Phosphorylation-inspired Design for Type I Collagen Biomimetic Remineralization

Li-sha Gu[1], **Jongryul Kim**[2], **Young Kyung Kim**[3], **Yan Liu**[4], **Sabine H. Dickens**[5], **David H. Pashley**[6], **Jun-qi Ling**[1,*], and **Franklin R. Tay**[6,7,*]

[1]Department of Operative Dentistry and Endodontics, Guanghua School of Stomatology, Sun Yat-sen University, Guangzhou, China

[2]Department of Conservative Dentistry, School of Dentistry, KyungHee University, Seoul, Korea

[3] Department of Conservative Dentistry, School of Dentistry, Kyungpook National University, Daegu, Korea

[4]Department of Stomatology, Tongji Hospital, Tongji Medical College, Huazhong University of Science and Technology, Wuhan, China

[5]American Dental Association Health Foundation, National Institute of Standards and Technology, Paffenbarger Research Center, Gaithersburg, Maryland, USA

[6]Department of Oral Biology, School of Dentistry, Medical College of Georgia, Augusta, Georgia, USA

[7]Department of Endodontics, School of Dentistry, Medical College of Georgia, Augusta, Georgia, USA

Abstract

Objectives—Type I collagen alone cannot initiate tissue mineralization. Sodium trimetaphosphate (STMP) is frequently employed as a chemical phosphorylating reagent in the food industry. This study examined the feasibility of using STMP as a functional analog of matrix phosphoproteins for biomimetic remineralization of resin-bonded dentin.

Methods—Equilibrium adsorption and desorption studies of STMP were performed using demineralized dentin powder (DDP). Interaction between STMP and DDP was examined using Fourier-transform infrared spectroscopy. Based on those results, a bio-inspired mineralization scheme was developed for chemical phosphorylation of acid-etched dentin with STMP, followed by infiltration of the STMP-treated collagen matrix with two etch-and-rinse adhesives. Resin-dentin interfaces were remineralized in a Portland cement-simulated body fluid system, with or without the use of polyacrylic acid (PAA) as a dual biomimetic analog. Remineralized resin-dentin interfaces were examined unstained using transmission electron microscopy.

Results—Analysis of saturation binding curves revealed the presence of irreversible phosphate group binding sites on the surface of the DDP. FT-IR provided additional evidence of chemical interaction between STMP and DDP, with increased in the peak intensities of the P=O and P–O–C

*Co-corresponding author: 1. Dr. Jun-qi Ling: Guanghua School of Stomatology, Sun Yat-sen University, 510080 Guangzhou/PR. China. Tel: +8620-83862558; Fax: +8620-83870412; lingjq@mail.sysu.edu.cn, 2. Dr. Franklin Tay: School of Dentistry, Medical College of Georgia, Augusta, Georgia, USA. Tel: (706) 7212031; Fax: (706) 7216252; ftay@mcg.edu.

stretching modes. Those peaks returned to their original intensities after alkaline phosphatase treatment. Evidence of intrafibrillar apatite formation could be seen in incompletely resin-infiltrated, STMP-phosphorylated collagen matrices only when PAA was present in the SBF.

Significance—These results reinforce the importance of PAA for sequestration of amorphous calcium phosphate nanoprecursors in the biomimetic remineralization scheme. They also highlight the role of STMP as a templating analog of dentin matrix phosphoproteins for inducing intrafibrillar remineralization of apatite nanocrystals within the collagen matrix of incompletely resin-infiltrated dentin.

Keywords

Adsorption; Sodium trimetaphosphate; Collagen; Dentin; Intrafibrillar remineralization

1. Introduction

Dental caries is a chronic infection in which hard tooth structures (enamel, dentin and cementum) are progressively broken down by bacteria, producing dental cavities. Tooth-colored resin-based composites have found increasing popularity for restoring dental cavities. The use of acid etching prior to the application of resin adhesives is a prerequisite for enhancing the mechanical retention of resin composites. However, exposed collagen fibrils remain within the bonded interface as a result of the discrepancy between the depths of acid demineralization and resin infiltration [1]. These naked collagen fibrils are prone to hydrolysis after water sorption [2]. Activation of endogenous matrix metalloproteinases (MMP) further results in breakdown of incompletely resin-infiltrated collagen matrices [3] and degradation of resin-dentin bonds [2,4].

As one of the most intriguing processes in nature [5], biomineralization is essential for the formation of hard tissues like bone and teeth. Dentin is a mineralized collagenous tissue formed by matrix-mediated mechanisms [6]. Collagen fibrils encapsulated by apatites in natural mineralized dentin do not degrade over time [7]. As contemporary tissue engineering technologies are not yet capable of creating artificial dentin, remineralization of incompletely resin-infiltrated dentin collagen matrices appears to be the logical approach for extending the longevity of resin-dentin bonds. Type I collagen, accounting for 90% of the total protein content in the organic matrix of dentin [8], provides the framework and spatial constraint for ordered crystal deposition [9]. However, in the absence of apatite seed crystallites, collagen by itself does not possess the thermodynamic and kinetic mechanisms for induction of apatite nucleation [10,11]. Acidic noncollagenous proteins (NCPs) promote nucleation and post-nucleation growth of apatite crystallites within and around the gap zones of collagen fibrils [12] and are essential for regulation of matrix mineralization [5,13].

Immobilization of protein molecules on intact collagen substrates promotes apatite nucleation because such molecules possess multiple polyanionic functional groups that act as favored sites for homogeneous nucleation [14]. The inductive effect of phosphoproteins on the formation of hydroxyapatite is a well known example [15]. Phosphophoryn, the major NCP present in dentin, has been shown to bind calcium ions with high affinity after its highly phosphorylated post-translational modification [11,16]. Grafting of molecules containing phosphate groups to polymeric biomaterials with limited or no mineralizing tendency has been reported as a successful procedure for converting those substrates into mineralized moieties [17,18]. Binding of biomimetic molecules containing multiple phosphate groups to collagen fibrils produces phosphorylated and negatively charged surfaces that attract calcium ions by electrostatic interaction. The phosphorylated collagen serves as a scaffold for homogeneous nucleation of

apatite crystallites [19]. This biomimetic process may, in part, recapitulate the function of phosphate groups in naturally-occurring phosphoproteins.

Trimetaphosphate (P_3m) derived from volcanic eruptions has a cyclic structure that contains three phosphorus atoms in a six-membered ring. It plays an important functional link in prebiotic chemistry due to its purported roles as a phosphorylation reagent for bioorganic compounds and a coupling reagent for oligomerization of amino acids and nucleosides [20-22]. Among its various salt forms, sodium trimetaphosphate (STMP, $Na_3P_3O_9$;Fig.1a) is commonly used in the food industry as a chemical phosphorylation reagent [23-25]. At alkaline pH, STMP can chemically react with the hydroxyl groups on proteins, thereby introducing phosphate functional groups to protein molecules [26]. Although there are ample examples of the application of STMP as an effective phosphorylation agent for edible plant proteins in the food industry, few studies have been conducted on its use on type I collagen, the major structural protein in bone and dentin. As a result, there is very limited understanding of the interactions between STMP and collagen and particularly its adsorption characteristics. A recent study that utilized STMP as a chemical phosphorylation agent for bovine collagen demonstrated extrafibrillar deposition of large spherical hydroxyapatite clusters around STMP-phosphorylated collagen matrices after the latter were incubated in a simulated body fluid (SBF) [26]. In that study, there was no sequestering mechanism, such as the use of polyaspartic acid or polyacrylic acid, for rendering the formation of apatite in a nanoscale [27,28]. The apatite clusters created in that study were large and could not fit inside collagen fibrils [26]. More importantly, in the absence of an amorphous calcium phosphate sequestering mechanism, the exact role played by STMP in inducing homogeneous nucleation of apatite within collagen fibrils (i.e. intrafibrillar mineralization) is unknown. While the binding of large apatite spherical clusters via STMP to collagen [26] may produce composite materials for filling of bone defects which can eventually be resorbed and replaced by new bone generated by osteocytes, those materials can not be used as a restorative material to replace dentin, as the latter is a non-regenerable substrate produced by terminally-differentiated odontoblasts. Thus, the use of STMP as a chemical phosphorylation agent for inducing *in-situ* mineralization of collagen fibrils appears to be a more pragmatic approach. However, in the absence of adjunctive polycarboxylic acid analogs as sequestering agents, the use of STMP alone as a collagen phosphorylaton agent has limited potential for in-situ remineralization of dentin in which the occurrence of intrafibrillar mineralization is perceived to be responsible for its biomechanical properties [29]. As the concentration of STMP employed for phosphorylating collagen has not been optimized in the previous study [26], examining the interaction between collagen and STMP and determining its optimal binding concentration will bring to fruition the more efficient use of STMP as a chemical phosphorylation agent for remineralization of dentin collagen matrices in the presence of additional biomimetic analogs with sequestering function.

Accordingly, equilibrium adsorption studies were first performed in the present study to identify the maximum STMP adsorption capacity on demineralized dentin collagen matrices. The STMP-phosphorylated demineralized dentin powder (DDP) at alkaline pH was also analyzed using Fourier transform-infrared spectroscopy (FT-IR). These data allow us to identify certain characteristics of the collagen matrix that are indicative of neo-phosphorylation. Both polyaspartic acid and polyacrylic acid (PAA) as carboxylic acid-containing polyelectrolytes have been employed as analogs of acidic NCPs such as dentin matrix protein 1 (DMP1) [30] for stabilizing and controlling the dimensions of amorphous phases in calcium carbonate and calcium phosphate precipitation systems [31]. Based on our previous studies on biomimetic remineralization using polyvinylphosphonic acid (PVPA) and PAA as dual analogs of NCPs [32-34], we used resin-dentin slab as a model for the design of a nanotechnology-inspired scheme for remineralizing incompletely resin-infiltrated demineralized dentin based on chemical phosphorylation of collagen with STMP and stabilization of amorphous nanoprecursors with PAA. Thus, the objective of this study was to

test the hypothesis that STMP is capable of binding irreversibly to collagen fibrils, producing the condition that favors homogeneous mineral induction and intrafibrillar remineralization in the presence of PAA-stabilized amorphous calcium phosphate nanophases.

2. Materials and methods

2.1 Preparation of DDP

One hundred and fifty extracted human third molars were obtained from anonymous subjects following their signed consent under a protocol approved by the Human Assurance Committee of the Medical College of Georgia. The teeth ground free of enamel, cementum and pulpal soft tissues were reduced to a fine powder by freezing the dentin in liquid nitrogen and triturating it in a stainless steel mixer mill at -120°C (Model MM301, Retsch, Newtown, PA, USA) for 10 min at 30 Hz. The dentin powder thus formed was sieved through multiple screens to exclude aggregates coarser than 38 μm in size. This fine powder was then completely demineralized in 0.2 M formic acid/sodium formate (pH = 2.96) containing MMP inhibitors at 4°C to prevent collagen degradation, with the end point of demineralization confirmed by using digital radiography. Thereafter, the DDP aliquots were filtered, washed three times with deionized water and lyophilized.

2.2 Adsorption of STMP on DDP

Equilibrium adsorption experiments were performed by contacting 50 mg of DDP with 1 mL of 82.7 mM STMP solution (Sigma-Aldrich, St. Louis, MO, USA) for 1 min, 5 min, 1 hr or 3 hr. Twelve different STMP solutions ranging from 0 (blank) to 30,000 mg/L (i.e. 3 mass%) were tested. Phosphorylation using STMP is pH-dependent [25]; more peptides are expected to be chemically phosphorylated at higher pH values. However, as collagen may be denatured at higher pH values, the STMP solution was adjusted to a pH of 9.5 using 5 M NaOH, enabling the highly cross linked dentin collagen fibrils to be phosphorylated under alkaline condition without denaturation.

After gentle agitation of the STMP-dentin powder mixtures at 37 °C for a designated time period, the reaction mixtures were centrifuged to retrieve the supernatant. The concentration of free STMP in each supernatant was deduced by measuring the corresponding phosphorous content [35]. Briefly, ammonium molybdate was used to react with phosphate to form a phosphomolybdate colored complex after 2 hr of incubation at 37°C. The latter was analyzed at 820 nm with a UV-VIS spectrophotometer. The concentration of unreacted STMP (R) in the supernatant was calculated using a linear regression equation derived from known STMP concentrations. The amount of bound STMP (B) was calculated by subtracting R from the initial STMP concentration.

Adsorption isotherms were derived based on the relationship between the STMP adsorbed per unit mass of dried demineralized dentin powder (mg/g) and the STMP concentration at equilibrium. The best fit isotherm model was established by statistically computing the R^2 values for the Langmuir and Freundlich isotherm models. The adsorption data were also analyzed by nonlinear regression curve-fitting (GraphPad, San Diego, CA, USA) by comparing a one-site versus a two-site specific binding model using the F-test. The two-site model was accepted if the fit was significantly better ($p < 0.05$) than that of the one-site model. Otherwise, the one-site model was accepted when it was not significantly different from the two-site model ($p > 0.05$). All measurements were repeated two to four times and the results were calculated as mean values from the parallel samples.

2.3 Desorption

Five different desorbents (water, 95% ethanol, 95% acetone, 130 mM NaCl and 500 mM NaCl) were examined. For each desorbent, the twelve STMP concentrations described previously were allowed to adsorb on DDP in a water-to-powder ratio of 1:0.05 for 3 hr, respectively. The DDP were then briefly washed with deionized water and re-suspended in 1 mL of the respective desorbent at 37 °C under mild agitation for 30 min or 24 hr. Subsequently, the supernatant was collected to determine the amount of STMP desorbed by analysis of the phosphorus content [35].

2.4 FT-IR

A Nicolet 6700 FT-IR spectrophotometer (Thermo Scientific Inc., Waltham, MA, USA) with a germanium attenuated total reflection (ATR) setup was used to collect FT-IR spectra from the powder before (control) and after 3 h immersion in the 2.5% STMP solution at pH 9.5. Infrared spectra were collected between 675-4000 cm^{-1} at 4 cm^{-1} resolution using 32 scans. To further examine if true chemical phosphorylation had occurred, the STMP-bound collagen was treated with 0.13 μg/mL alkaline phosphatase (Sigma-Aldrich) for 6 hr at 37°C. After rinsed three times in deionized water, the enzyme treated STMP-sorbed DDP was re-subjected to FT-IR analysis.

2.5 Dentin bonding and STMP pre-treatment

Twenty additional third molars were collected abiding by the aforementioned human assurance protocol. A mid-coronal flat dentin surface was prepared perpendicular to the longitudinal axis of each tooth using an Isomet diamond saw (Buehler Ltd, Lake Bluff, IL, USA) under water-cooling. The occlusal dentin surface was polished with a 320-grit silicon carbide paper under running water to create an enamel-free bonding surface. Each dentin surface was etched with 37% phosphoric acid (Bisco Inc. Schaumburg, IL, USA) for 15 sec to create a 5-8 μm thick zone of completely demineralized dentin on top of a mineralized dentin base. After rinsing with deionized water, a STMP solution with optimal concentration derived from the adsorption results was applied to the etched dentin for 5 min using mild agitation.

Two etch-and-rinse dentin adhesives were used (N=10): One-Step (Bisco Inc), an acetone-based unfilled adhesive, and XP Bond (Dentsply De Trey, Konstanz, Germany), a tertiary butanol-based filled adhesive. Each adhesive was applied to the STMP-primed dentin and light-polymerized for 20 sec. This was followed by incremental placement of two 2-mm thick layers of a resin composite. The bonded teeth were stored at 100% relative humidity for 24 h to enable the bonds to mature. Each tooth was then sectioned occluso-gingivally into 1 mm thick slabs containing the resin-dentin interface. Two central slabs from each tooth were selected for the study, one slab for the control group and the other slab for the experimental group.

2.6 Remineralization medium

White Portland cement (Lehigh Cement Company, Allentown, Pennsylvania, USA) was mixed with deionized water in a water-to-powder ratio of 0.35:1, placed in flexible silicone molds and incubated at 100% relative humidity for one week before use. The SBF was prepared by dissolving 136.8 mM NaCl, 4.2 mM $NaHCO_3$, 3.0 mM KCl, 1.0 mM $K_2HPO_4{\cdot}3H_2O$, 1.5 mM $MgCl_2{\cdot}6H_2O$, 2.5 mM $CaCl_2$ and 0.5 mM Na_2SO_4 in deionized water [36] and adding 3.08 mM sodium azide to prevent bacterial growth. This SBF served as the control remineralization medium, which contained no biomimetic analog. For the biomimetic remineralization medium, 500 μg/mL of PAA (Mw = 1,800; Sigma-Aldrich, St. Louis, Illinois, USA) was added to the SBF as a biomimetic analog.

2.7 Biomimetic remineralization

Each 1 mm thick slab of resin-bonded dentin was placed on top of a set Portland cement block (*ca*. 1 g) inside a glass scintillation vial. The latter was filled with 15 mL of SBF for the control or 15 mL of the biomimetic remineralization medium for the experimental specimens. Each capped vial was incubated at 37 °C. The media were changed every month, with their pH monitored weekly so that they were above 9.5. This ensured that the collagen fibrils were chemically phosphorylated in the presence of STMP under alkaline conditions [22], and that apatite was formed instead of octacalcium phosphate [37]. Experimental and control specimens were retrieved after 1-4 months for ultrastructural examination of the extent of remineralization.

2.8 Transmission electron microscopy (TEM)

The specimen slices were dehydrated in an ascending series of ethanol (50-100%), immersed in propylene oxide as a transitional fluid and embedded in epoxy resin [32]. Non-demineralized, epoxy resin-embedded 90 nm thick sections were prepared and examined without further staining using a JEM-1230 transmission electron microscope (JEOL, Tokyo, Japan) operated at 110 kV.

3. Results

3.1 Adsorption isotherms and modeling

Figure 1b represents the adsorption isotherms of STMP on DDP after 1 min, 5 min, 1 hr and 3 hr. For each time period, there was an increase in the amount of sorbed STMP with the 0-30,000 mg/L range. The amount of sorbed STMP increased with the time of contact with DDP, although more than 90% of the STMP was adsorbed to the DDP within the first 5 min. Non-linear curve fitting of the resulting plots suggested that the one-site specific binding model was preferred ($p < 0.05$) over the two-site specific binding model. Table I shows the best-fit parameters generated from nonlinear regression of the experimental data using the one-site specific binding model. Figure 2 shows linear plots of the adsorption data with sorbate concentrations, based on the Langmuir (Fig. 2a) and Freundlich adsorption models (Fig. 2b). A summary of the isotherm constants and correlation for the Langmuir and Freundlich isotherms is presented in Table II. Both the R^2 values obtained for the Langmuir and Freundlich expressions were highly significant ($p < 0.01$).

3.2 Desorption isotherms

Desorption isotherms of STMP in the presence of different solvents are shown in Fig.3. These isotherms were compared with the maximum adsorption isotherm of STMP at 3 hr. Organic solvents (i.e. 95% ethanol and 95% acetone) were ineffective in displacing STMP from the STMP-sorbed DDP. When different concentrations (0 to 0.5 M) of aqueous NaCl solutions were used as desorbents, only partial desorption was observed up to 24 hr. Moreover, desorption of STMP from demineralized dentin collagen was unaltered by the presence of 0.13-0.5 M NaCl when compared to the desorption characteristics of STMP in deionized water (Fig.3). With increasing STMP concentration, the percentage of desorbed STMP decreased, resulting in a higher amount of bound STMP.

3.3 FT-IR

Figure 4 represents the IR spectra generated from DDP before and after immersion in an alkaline 2.5 mass% STMP solution (pH = 9.5) for 3 hr. Prior to STMP treatment, the completely demineralized dentin collagen matrix (Fig.4, spectrum DDP) revealed characteristic collagen related bands amide I, II and III at 1200-1700 cm^{-1} [38]. Since the DDP was tested under hydrated condition, the amide A and B bands located at 2900-3400 cm^{-1} were overlapped with

the broad water sorption band (2500-3700 cm^{-1}) representing the $\upsilon_1\upsilon_3$OH stretching mode of adsorbed water molecules [39]. As a result, a faint amide B band was seen in the spectrum DDP in Fig.4. The FT-IR profile of DDP after 3 hr immersion in 2.5 mass% STMP at pH 9.5 is depicted in spectrum S-DDP. When compared with the baseline DDP spectrum, no change in the amide peaks was observed. However, the intensities of the peaks related to the P=O and P–O–C stretching modes at 1080, 1030, 1010 and 976 cm^{-1} increased after STMP treatment (Fig.4, spectrum S-DDP) [40-42], and subsequently returned to their original intensities after alkaline phosphatase treatment (Fig.4, spectrum A-S-DDP). These changes were not apparent when the STMP solution was not adjusted to an alkaline pH prior to reaction (not shown).

3.4 TEM

3.4.1 Control specimens—Control specimens retrieved after 4 months exhibited no remineralization within the adhesive resin-infiltrated demineralized collagen matrix (Fig. 5a), despite the presence of 0.3-0.5 μm diameter electron-dense clusters within the resin composite and collagen matrices. A high magnification view of the electron-dense clusters revealed that they were deposits of mineral aggregates (Fig. 5b).

3.4.2 Experimental Specimens—At an early stage of remineralization, electron-dense globular droplets were identified in the resin-infiltrated demineralized collagen matrices (Fig. 6a). They were predominantly located adjacent to the dentin bonding surface with a few scattered within the interior of resin-infiltrated demineralized dentin. Figure 6b shows an intermediate stage of remineralization in which very fine electron-dense strands could be discerned through the entire interdiffusion zone. With a more mature stage of biomimetic remineralization, electron-dense collagen fibrils could be seen within the demineralized dentin (Figs 6c and 6d). As the spaces between the collagen fibrils were occupied by resin, remineralization was predominantly identified within the fibrils (i.e. intrafibrillar remineralization).

Figures 7 and 8 are high magnification images representative of the resin-infiltrated demineralized collagen matrices after 1-4 months immersion in the PAA-supplemented remineralization medium. Figure 7a represents a high magnification view of the junction between the adhesive and the dentin surface depicted in Fig. 6a, showing the presence of various sizes of electron-dense, globular droplets within the demineralized dentin at an early stage of remineralization. The larger droplets appeared to be formed by the fusion of multiple smaller droplets (Fig. 7a). Moreover, some electron-dense microfibrillar strands could be identified within the demineralized collagen fibrils, with the occasional appearance of amorphous, electron-dense globular droplets adjacent to the braided fibrils (Fig. 7a). At this stage, remineralization appeared as continuous, braided electron-dense extensions following the microfibrillar arrangement of collagen fibrils (Fig. 7b). Diffuse selected area electron diffraction patterns derived from the electron-dense strands (Fig. 7b, inset) indicated the absence of crystalline phases within these regions. With a more mature stage of biomimetic remineralization, transformation of the continuous, braided mineral phase into discrete, non-overlapping mineral platelets could be seen within a single collagen fibril (Figs.7c, 8b and 8c). These non-overlapping mineral platelets were ultimately converted to larger overlapping platelets or needles (Figs.7d and 8d), representing an advanced stage of remineralization. These apatite nanocrystals were oriented along the longitudinal axes of the microfibrils, enabling the rope-like subfibrillar architecture [43] of the collagen fibrils to be discerned (Figs.7c, 7d, and 8b-8d). Diffuse selected area electron diffraction ring patterns collected from these mineral platelets were characteristic of polycrystalline apatite (Fig. 8d, inset).

4. Discussion

4.1 Adsorption characteristics of STMP

The Langmuir [44] and Freundlich [45] sorption models were employed to examine the relationship between sorbed (q_e) and aqueous STMP concentrations (C_e) at equilibrium. The adsorption equilibrium isotherms shown in Fig.1 were transformed into the linear forms of the Freundlich and Langmuir isotherms (Eqs. (1) and (2)) and analyzed using linear regression analyses. The linear plots yielding giving an R^2 value closest to unity were deemed to provide the best fit.

The linearized form of the Langmuir expression is represented by Eq.(1):

$$C_e/q_e=1/(q_0K_L)+C_e/q_0 \quad \text{Eq.(1)}$$

where q_0 and K_L are the Langmuir constants. The capacity of STMP in binding to dentin collagen matrices was determined by plotting C_e/q_e against C_e using the above equation. As shown in Fig.2a, the Langmuir isotherm appears to provide an acceptable model of the sorption characteristics. This model describes sorption onto specific homogeneous sites within a sorbent, and predicts the existence of monolayer coverage of the sorbate (STMP) at the outer surface of the sorbent (collagen). Once the sorbate molecule occupies a site, no further adsorption can take place at that site. The Langmuir equation is based on the assumption of a structurally homogeneous sorbent (collagen) where all sorption sites are identical and energetically equivalent and there is no interaction between molecules adsorbed on neighboring sites.

Freundlich isotherm is the result of overlapping patterns of several Langmuir-type adsorption curves occurring at different sites on a complex sorbent surface. The same set of equilibrium data were further analyzed using the linearized form of the Freundlich equation:

$$\ln q_e=\ln K_F+1/n_F \ln C_e \quad \text{Eq.2}$$

where K_F and n_F are the Freundlich constants. As shown in Fig.2b, the plot of ln q_e versus ln C_e was linear, indicating a good correlation with respect to the Freundlich isotherm. This model assumes that there are many types of sites acting simultaneously, each with a different free energy of sorption, and that there is a large amount of available sites [46].

Based on the coefficients of determination (Table II), the R^2 values obtained using the Freundlich model and the Langmuir model were both highly significant. Thus, the sorption equilibrium isotherms for STMP were further analyzed by non-linear curve fitting analysis. The results suggested that STMP binding is more compliant with the classical Langmuir-type binding model (i.e. one-site specific binding model), as represented by the Eq.(3).

$$Y=B_{max}X/(K_d+X) \quad \text{Eq.(3)}$$

where X is the concentration of free STMP in equilibrium, B_{max} is the maximum binding capacity and K_d is the dissociation constant (i.e. the reciprocal of the association constant K_a) [47]. Excellent curve fitting were obtained (Fig.1) and represented by the R^2 values in Table II. That is, STMP appears to bind to type I collagen and result in localization of the initial

apatite crystallites on specific sites along the collagen fibrils. As the adsorption isotherm data suggests that sorption of STMP onto DDP reaches equilibrium at 2.5 mass% STMP, this concentration was employed for the rest of the study.

4.2 Irreversible binding of STMP

Results from the present study indicated that the STMP was irreversibly bound to dentin collagen and that little STMP was eluted when 95% ethanol or 95% acetone was used as desorbents, both of which represent common solvents employed in dentin adhesives. This may probably be ascribed to the insolubility of STMP in ethanol and acetone. The effects of 0.13 M and 0.5 M NaCl on STMP desorption provided the first evidence on its chemical interaction with demineralized dentin collagen. If the sorption of STMP is the result of electrostatic interaction, desorption would have increased with increasing salt concentration that competes with the STMP molecules for electrostatic binding sites. However, the amount of STMP debinding from the STMP-sorbed collagen was independent of the NaCl concentration. As ionic interactions are weakened by increasing ionic strength [48], it may be concluded that electrostatic binding is not the main interaction between STMP and dentin collagen. Conversely, binding is likely to be a result of covalent bonding between STMP and the collagen molecules.

4.3 Mechanism of binding of STMP to demineralized dentin collagen

Dentin contains numerous NCPs, among which dentin matrix protein 1 (DMP 1) has been shown to bind specifically to fibrillar collagen with high affinity [49]. Although the aforementioned isotherm models provide a possible explanation of irreversible binding of STMP to demineralized dentin collagen, it does not explicitly incorporate a mechanism for collagen phosphorylation within the peptide chains. The FT-IR results of the present study provides direct vibrational evidence that chemical phosphorylation of the dentin collagen occurs following the use of STMP under alkaline condition, possibly via phosphoesterification of the hydroxyl amino acids in the collagen molecules. It has been shown that the STMP is hydrolyzed into sodium tripolyphosphate (STP) in alkaline solutions [50]. The mechanism is assumed to proceed by opening of the STMP six-membered ring by the hydroxyl group of sodium hydroxide (NaOH). The STP, which has three phosphate groups, would subsequently create covalent bonding between the phosphate groups and hydroxyl group-containing amino acids on the side chains of the collagen molecules [51]. It has been previously reported that the free hydroxyl groups in the protein molecules exhibit high reactivity only under alkaline conditions of pH > 9 [51]. As a high pH value may result in denaturation of collagen [52] while a lower pH value may not be sufficient for initiating the phosphorylation reaction, control of pH is critical during collagen phosphorylation with STMP. Based on our FT-IR results, no changes could be discerned from the collagen amide peaks after chemical phosphorylation (Fig.4). In particular, the amide I band (C=O stretching vibration) at 1600-1700 cm^{-1}, which is sensitive to the molecular conformation of the polypeptide chains [53], remained unaltered. The resultmay be explained by the fact the dentin collagen is highly cross-linked, thus minimizing its denaturation under moderately alkaline conditions. This permits amino acids containing OH groups in their side chains (serine, threonine and tyrosine) to be chemically phosphorylated to form phosphoester bonds through the attachment of phosphate groups to the oxygen of seryl, threonyl and tyrosyl residues [23]. The STMP immobilized on the collagen surface after chemical phosphorylation may serve as templates for the attraction of amorphous calcium phosphate nanoprecursors that are initially presented as sequestered, PAA-stabilized liquid-like droplets [31].

4.4 Biomimetic remineralization of STMP phosphorylated demineralized dentin

Based on the STMP adsorption data, a 5-min STMP application time was adopted for chemical phosphorylation of acid-etched dentin in the present remineralization scheme. The results obtained from the control specimens demonstrated that intrafibrillar remineralization of STMP pre-treated demineralized dentin did not occur when PAA was absent from the remineralization medium. However, calcium phosphate deposits about 0.3 to 0.5 μm in diameter were identified within the voids of composite resins as well as the phosphorylated dentin collagen matrices after aging. This finding is consistent with the result of a recent investigation [26], on the formation of calcium phosphate microspheres (about 1 μm in diameter) on the surface STMP-phosphorylated collagen after its immersion in SBF. These calcium phosphate deposits are large in size and are unlikely to fit into the gap zones of collagen fibrils with a diameter of about 100 nm. By contrast, when the STMP pre-treated specimens were incubated in PAA-supplemented SBF in the present study, apatite nanocrystals were observed and intrafibrillar remineralization was successfully achieved within incompletely resin-infiltrated collagen matrices. Addition of PAA to the Portland cement/SBF system has been shown to be essential for the stabilization of the amorphous calcium phosphate (ACP) precursors released by the interaction between set Portland cement and SBF to a nanoscale in our previous study [54]. Presumably, the low molecular weight PAA functions as a surfactant [55], permitting liquid-liquid phase separation of the ACP nanoprecursors from the aqueous remineralization medium [56], thereby sequestering the ACP phases into liquid nanodroplets. This sequestration step can prevent the nanoprecursors from aggregation and precipitation [55], rendering them small enough to penetrate a demineralized collagen matrix followed by their transformation into apatite nanocrystals during the course of biomineralizaiton. More recent studies suggested that these fluidic nanoprecursors may be the result of the aggregation of even smaller (0.6-1.1 nm) amorphous prenucleation ionic clusters [57,58]. This finding highlights the role of PAA in the nanotechnology-inspired biomimetic remineralization scheme.

Bone and/or dentin-specific NCPs, as polyanionic protein molecules, are believed to bind to the collagen substrate at specific sites such as gap regions and pores of the fibrillar assembly [59,60]. The bound proteins present anionic charge sites and thus possess high calcium binding capacity [61,62]. Considerable evidence suggests an active regulatory role for NCPs during biomineralization process [63]. As a biomimetic analog of NCPs, the phosphate groups of STMP anions presumably adsorb to the collagen surface and form covalent bonds with the latter under an alkaline pH. The phosphorylated collagen results in a highly negative charged surface, acting as a virtual sink for the binding of calcium ions [64]. The latter may subsequently be absorbed onto the surface of the phosphorylated collagen by electrostatic forces, and eventually precipitate to form calcium phosphate clusters. These clusters will grow until they coalesce with adjacent clusters into apatitic nuclei. It has been suggested that phosphorylation may change the conformation of the protein [65], exposing anionic domains on the collagen surface that can interact with calcium on the apatite surface. Thus, bound STMP may also function as a template for apatite nucleation within the collagen fibril.

Lowenstam and Weiner [66] previously that carbonated apatite in mineralized tissues is formed via an ACP precursor phase. A growing body of evidence has accumulated in recent years indicating that large single-crystal biominerals are not formed from their ion constituents but from amorphous precursor phases [67,68]. Consistent with previous findings, we have been able to observe electron-dense, globular droplets congregating around the periphery of collagen fibrils at an early stage of bioremineralization (Fig.7a) followed by transformation into continuous braided mineral phase (Fig.7b) and discrete nanocrystal platelets (Figs.7c, 7d, 8b-8d) within the collagen fibrils over time. It is conceived that these processes are integrated during the biomineralization of apatite crystallites [57].

Collectively, our results indicate that the STMP molecules can bind to demineralized collagen fibrils following direct application, thereby guiding the deposition of PAA-stabilized ACP nanoprecursors within the dentin collagen fibrils. In the present study, the STMP solution applied to the acid-etched dentin surface was at its original pH (pH = 5.69) without an addition of NaOH. Based on our previous finding, the pH value of the present Portland cement/SBF system rises rapidly to its maximum pH (about pH 11) within the first 24 hours [69]. Thus, it is reasonable to assume that after application of the adhesive resin, the STMP molecules embedded in the resin-collagen complex are transformed into STP via alkaline hydrolysis [50]. During tooth development, the most abundant of the NCPs in dentin, phosphophoryn, is deposited directly at the advancing mineralization front of dentin [70]. Conversely, in the present study, STMP was applied on the acid-etched dentin surface under diffusional control. This challenging issue should be considered in future designs of biomimetic delivery systems for remineralizing caries-affected dentin which may be more than 100 μm thick [71].

5. Conclusions

Adsorption isotherms of STMP onto DDP were consistent with both Langmuir and Freundlich models. Non-linear curve fitting also demonstrated that the one-site specific binding model fit the adsorption equilibrium data well in the examined concentration range. The desorption efficiency obtained with NaCl (0.13 or 0.5 M) as desorbents was low and comparable to that obtained using water, indicating sorption of STMP on DDP may be primarily attributed to covalent bonding between the STMP and collagen molecules. Based on the TEM results, formation of apatite crystallites within the collagen fibrils appears to be critically dependent on the addition of STMP and PAA in the biomimetic process. In particular, STMP may provide the interfacial linkage between mineral crystallites and collagen fibrils, and serves as a biomimetic analog for the formation of mineralized collagen fibrils. The phosphate groups of STMPs immobilized on the collagen fibrils are thought to contribute as binding sites for calcium ions, and play a direct role in the process of apatite nucleation onto collagen. Once apatite is nucleated, it can grow spontaneously from PAA-stabilized ACP nanoprecursors in the simulated body environment until the nucleus becomes a single apatite platelet. Collectively, STMP functions as an initiator for apatite nucleation *in vitro* and generates calcium phosphate deposits with a morphology that mimics the crystals found at the mineralization front of bone and dentin. These results provide new insights into basic mechanisms of collagen mineralization, and can lead to the development of a clinically-applicable delivery system by incorporating both biomimetic analogs (i.e. STMP and PAA) into the steps involved in the application of the adhesives and filling materials. Moreover, understanding the sorption mechanisms involved and molecular recognition for STMP would allow future applications to other collagen matrices such as bone collagen or reconstituted collagen scaffolds by understanding the amino acid residues in dentin collagen that are responsible for STMP-collagen affinity.

Acknowledgments

This study was supported by Grant R21 DE019213-01 from the National Institute of Dental and Craniofacial Research (PI. Franklin R. Tay). We thank Michelle Barnes for secretarial support.

References

1. Sano H, Shono T, Takatsu T, Hosoda H. Microporous dentin zone beneath resin-impregnated layer. Oper Dent 1994;19:59–64. [PubMed: 8008612]
2. Hashimoto M, Ohno H, Sano H, Kaga M, Oguchi H. In vitro degradation of resin-dentin bonds analyzed by microtensile bond test, scanning and transmission electron microscopy. Biomaterials 2003;24:3795–3803. [PubMed: 12818552]

3. Pashley DH, Tay FR, Yiu C, Hashimoto M, Breschi L, Carvalho RM, et al. Collagen degradation by host-derived enzymes during aging. J Dent Res 2004;83:216–221. [PubMed: 14981122]
4. De Munck J, Van Meerbeek B, Yoshida Y, Inoue S, Vargas M, Suzuki K, et al. Four-year water degradation of total-etch adhesives bonded to dentin. J Dent Res 2003;82:136–140. [PubMed: 12562888]
5. Lowenstam, HA.; Weiner, S. On Biomineralization. New York: Oxford University Press; 1989. p. 324New York, NY, USA
6. George A, Srinivasan R, Thotakura S, Veis A. The phosphophoryn gene family: identical domain structures at the carboxyl end. Eur J Oral Sci 1998;106:221–226. [PubMed: 9541229]
7. Carrilho MR, Tay FR, Pashley DH, Tjäderhane L, Carvalho RM. Mechanical stability of resin-dentin bond components. Dent Mater 2005;21:232–241. [PubMed: 15705430]
8. Weiner S, Wagner HD. The material bone: Structure mechanical function relations. Annu Rev Mater Sci 1998;28:271–298.
9. Veis A. Mineral-matrix interactions in bone and dentin. J Bone Miner Res 1993;8:S493–497. [PubMed: 8122518]
10. Saito T, Arsenault AL, Yamauchi M, Kuboki Y, Crenshaw MA. Mineral induction by immobilized phosphoproteins. Bone 1997;21:305–311. [PubMed: 9315333]
11. Saito T, Yamauchi M, Abiko Y, Matsuda K, Crenshaw MA. In vitro apatite induction by phosphophoryn immobilized on modified collagen fibrils. J Bone Miner Res 2000;15:1615–1619. [PubMed: 10934661]
12. Hoshi K, Ejiri S, Ozawa H. Organic components of crystal sheaths in bones. J Electron Microsc (Tokyo) 2001;50:33–40. [PubMed: 11291958]
13. Veis, A. The role of acidic proteins in biological mineralization. In: Everett, DH.; Vincent, G., editors. Ions in Macromolecular and Biological Systems. Vol. 29. Scientechnia; Bristol, UK: 1978. p. 259-267.
14. Tanahashi M, Matsuda T. Surface functional group dependence on apatite formation on self-assembled monolayers in a simulated body fluid. J Biomed Mater Res 1997;34:305–315. [PubMed: 9086400]
15. Banks E, Nakajima S, Shapiro LC, Tilevitz O, Alonzo JR, Chianelli RR. Fibrous apatite grown on modified collagen. Science 1977;198:1164–1166. [PubMed: 929194]
16. Hunter GK, Goldberg HA. Modulation of crystal formation by bone phosphoproteins: role of glutamic acid-rich sequences in the nucleation of hydroxyapatite by bone sialoprotein. Biochem J 1994;302:175–179. [PubMed: 7915111]
17. Li S, Liu Q, de Wijn J, Wolke J, Zhou B, de Groot K. In-vitro apatite formation on phosphorylated bamboo. J Mater Sci Mater Med 1997;8:543–549. [PubMed: 15348706]
18. Yokogawa Y, Paz Reye J, Mucalo MR, Toriyama M, Kawamoto Y, Suzuki T, et al. Growth of calcium phosphate on phosphorylated chitin fibres. J Mater Sci Mater Med 1997;8:407–412. [PubMed: 15348722]
19. Hartgerink JD, Beniash E, Stupp SI. Self-assembly and mineralization of peptide-amphiphile nanofibers. Science 2001;294:1684–1688. [PubMed: 11721046]
20. Inoue H, Baba Y, Furukawa T, Maeda Y, Tsuhako M. Formation of dipeptide in the reaction of amino acids with cyclo-triphosphate. Chem Pharm Bull 1993;41:1895–1899.
21. Rabinowitz J, Flores J, Krebsbach R, Rogers G. Peptide formation in the presence of linear or cyclic polyphosphates. Nature 1969;224:795–796. [PubMed: 4188388]
22. Schwartz AW. Specific phosphorylation of the 2- and 3- positions in ribonucleosides. J Chem Soc Chem Commun 1969;23:1393.
23. Zhang K, Li Y, Ren Y. Research on the phosphorylation of soy protein isolate with sodium tripolyphosphate. J Food Eng 2006;79:1233–1237.
24. Matheis G, Whitaker JR. Chemical phosphorylation of food proteins: an overview and a prospectus. J Agric Food Chem 1984;32:699–705.
25. Lee SH, Yang JI, Hong SM, Hahm DH, Lee SY, Kim IH, et al. Phosphorylation of peptides derived from isolated soybean protein: effects on calcium binding, solubility and influx into Caco-2 cells. Biofactors 2005;23:121–128. [PubMed: 16410634]

26. Li X, Chang J. Preparation of bone-like apatite-collagen nanocomposites by a biomimetic process with phosphorylated collagen. J Biomed Mater Res A 2008;85:293–300. [PubMed: 17688292]
27. Deshpande AS, Beniash E. Bio-inspired synthesis of mineralized collagen fibrils. Cryst Growth Des 2008;8:3084–3090.
28. Liou SC, Chen SY, Liu DM. Synthesis and characterization of needlelike apatitic nanocomposite with controlled aspect ratios. Biomaterials 2003;24:3981–3988. [PubMed: 12834593]
29. Bertassoni LE, Habelitz S, Kinney JH, Marshall SJ, Marshall GW Jr. Biomechanical perspective on the remineralization of dentin. Caries Res 2009;43:70–77. [PubMed: 19208991]
30. He G, Gajjeraman S, Schultz D, Cookson D, Qin C, Butler WT, Hao J, George A. Spatially and temporally controlled biomineralization is facilitated by interaction between self-assembled dentin matrix protein 1 and calcium phosphate nuclei in solution. Biochemistry 2005;44:16140–16148. [PubMed: 16331974]
31. Olszta MJ, Odom DJ, Douglas EP, Gower LB. A new paradigm for biomineral formation: mineralization via an amorphous liquid-phase precursor. Connect Tissue Res 2003;44 1:326–334. [PubMed: 12952217]
32. Tay FR, Pashley DH. Guided tissue remineralisation of partially demineralised human dentine. Biomaterials 2008;29:1127–1137. [PubMed: 18022228]
33. Tay FR, Pashley DH. Biomimetic remineralization of resin-bonded acid-etched dentin. J Dent Res 2009;88:719–724. [PubMed: 19734458]
34. Mai S, Kim YK, Toledano M, Breschi L, Ling JQ, Pashley DH, et al. Phosphoric acid esters cannot replace polyvinylphosphonic acid as phosphoprotein analogs in biomimetic remineralization of resin-bonded dentin. Dent Mater 2009;25:1230–1239. [PubMed: 19481792]
35. Chen PS, Toribara TY, Warner H. Microdetermination of phosphorus. Anal Chem 1956;28:1756–1758.
36. Kokubo T, Kushitani H, Sakka S, Kitsugi T, Yamamuro T. Solutions able to reproduce in vivo surface-structure changes in bioactive glass-ceramic A-W. J Biomed Mater Res 1990;24:721–734. [PubMed: 2361964]
37. Meyer JL, Eanes ED. A thermodynamic analysis of the secondary transition in the spontaneous precipitation of calcium phosphate. Calcif Tissue Res 1978;25:209–216. [PubMed: 30523]
38. Chang MC, Tanaka J. FT-IR study for hydroxyapatite/collagen nanocomposite cross-linked by glutaraldehyde. Biomaterials 2002;23:4811–4818. [PubMed: 12361620]
39. Bachmann L, Baffa O, Zezell DM. Thermal degradation of dentin collagen evaluated with ESR, infrared and optical spectroscopy. Philos Mag 2007;87:1033–1042.
40. Leone G, Torricelli P, Giardino R, Barbucci R. New phosphorylated derivatives of carboxymetylcellulose with osteogenic activity. Polymer Adv Tech 2008;19:824–830.
41. Ishii K, Yanase K, Suzuki S, Yamamoto M, Chihara K, Tabata Y, et al. Phosphorylation analysis using FT-IR and the application for an evaluation of biomaterials. J Jpn Soc Infrared Sci Technol 2004;14:44–50.
42. Hayakawa T, Yoshinari M, Sakae T, Nemoto K. Calcium phosphate formation on the phosphorylated dental bonding agent in electrolyte solution. J Oral Rehabil 2004;31:67–73. [PubMed: 15125600]
43. Bozec L, van der Heijden G, Horton M. Collagen fibrils: nanoscale ropes. Biophys J 2007;92:70–75. [PubMed: 17028135]
44. Langmuir I. The adsorption of gas, mica and platinium. J Am Chem Soc 1918;40:1361.
45. Freundlich, H. Colloid and capillary chemistry. London: Metheum; 1926. p. 883
46. Garcia-Zubiri IX, Gonzalez-Gaitano G, Isasi JR. Sorption models in cyclodextrin polymers: Langmuir, Freundlich, and a dual-mode approach. J Colloid Interface Sci 2009;337:11–18. [PubMed: 19501834]
47. Bothwell MK, Walker LP. Evaluation of parameter estimation methods for estimating cellulase binding constants. Biores Technol 1995;53:21–29.
48. Kyriacou A, Neufeld RJ, Mackenzie CR. Reversibility and competition in the adsorption of Trichoderma reesei cellulase components. Biotechnol Bioeng 1989;33:631–637. [PubMed: 18587961]

49. He G, George A. Dentin matrix protein 1 immobilized on type I collagen fibrils facilitates apatite deposition in vitro. J Biol Chem 2004;279:11649–11656. [PubMed: 14699165]
50. Shen CY. Alkaline hydrolysis of sodium trimetaphosphate in concentrated solutions and its role in built detergents. Ind Eng Chem Prod Res Dev 1966;5:272–276.
51. Ferrel Sung HY. Chemical phosphorylation of food proteins by sodium trimetaphosphate. J Food Sci 1982;47:716–724.
52. Ni F, Sun S, Huang C, Zhao Y. N-phosphorylation of amino acids by trimetaphosphate in aqueous solution—learning from prebiotic synthesis. Green Chem 2009;11:569–573.
53. Spencer P, Wang Y, Katz JL, Misra A. Physicochemical interactions at the dentin/adhesive interface using FTIR chemical imaging. J Biomed Opt 2005;10:031104. [PubMed: 16229629]
54. Kim JR, Arola DD, Gu LS, Kim YK, Mai S, Pashley DH, Tay FR. Functional biomimetic analogs help remineralize partially-demineralized resin-infiltrated dentin collagen matrices via a bottom-up approach. Acta Biomater. in press.
55. Liou SC, Chen SY, Liu DM. Manipulation of nanoneedle and nanosphere apatite/poly(acrylic acid) nanocomposites. J Biomed Mater Res B Appl Biomater 2005;73:117–122. [PubMed: 15672405]
56. Gower LB. Biomimetic model systems for investigating the amorphous precursor pathway and its role in biomineralization. Chem Rev 2008;108:4551–4627. [PubMed: 19006398]
57. Pouget EM, Bomans PH, Goos JA, Frederik PM, de With G, Sommerdijk NA. The initial stages of template-controlled CaCO3 formation revealed by cryo-TEM. Science 2009;323:1455–1458. [PubMed: 19286549]
58. Gebauer D, Volkel A, Cölfen H. Stable prenucleation calcium carbonate clusters. Science 2008;322:1819–1822. [PubMed: 19095936]
59. Linde A, Goldberg M. Dentinogenesis. Crit Rev Oral Biol Med 1993;4:679–728. [PubMed: 8292714]
60. Landis WJ, Hodgens KJ, Song MJ, Arena J, Kiyonaga S, Marko M, et al. Mineralization of collagen may occur on fibril surfaces: evidence from conventional and high-voltage electron microscopy and three-dimensional imaging. J Struct Biol 1996;117:24–35. [PubMed: 8776885]
61. Chen Y, Bal BS, Gorski JP. Calcium and collagen binding properties of osteopontin, bone sialoprotein, and bone acidic glycoprotein-75 from bone. J Biol Chem 1992;267:24871–24878. [PubMed: 1447223]
62. Wallwork ML, Kirkham J, Chen H, Chang SX, Robinson C, Smith DA, et al. Binding of dentin noncollagenous matrix proteins to biological mineral crystals: an atomic force microscopy study. Calcif Tissue Int 2002;71:249–255. [PubMed: 12154396]
63. Sreenath T, Thyagarajan T, Hall B, Longenecker G, D'Souza R, Hong S, et al. Dentin sialophosphoprotein knockout mouse teeth display widened predentin zone and develop defective dentin mineralization similar to human dentinogenesis imperfecta type III. J Biol Chem 2003;278:24874–24880. [PubMed: 12721295]
64. Linde A, Lussi A, Crenshaw MA. Mineral induction by immobilized polyanionic proteins. Calcif Tissue Int 1989;44:286–295. [PubMed: 2501010]
65. Lahiri SD, Zhang G, Dunaway-Mariano D, Allen KN. Caught in the act: the structure of phosphorylated beta-phosphoglucomutase from Lactococcus lactis. Biochemistry 2002;41:8351–8459. [PubMed: 12081483]
66. Lowenstam HA, Weiner S. Transformation of Amorphous Calcium Phosphate to Crystalline Dahillite in the Radular Teeth of Chitons. Science 1985;227:51–53. [PubMed: 17810022]
67. Weiner S, Sagi I, Addadi L. Structural biology. Choosing the crystallization path less traveled Science 2005;309:1027–1028.
68. Politi Y, Arad T, Klein E, Weiner S, Addadi L. Sea urchin spine calcite forms via a transient amorphous calcium carbonate phase. Science 2004;306:1161–1164. [PubMed: 15539597]
69. Tay FR, Pashley DH, Rueggeberg FA, Loushine RJ, Weller RN. Calcium phosphate phase transformation produced by the interaction of the portland cement component of white mineral trioxide aggregate with a phosphate-containing fluid. J Endod 2007;33:1347–1351. [PubMed: 17963961]
70. Weinstock M, Leblond CP. Radioautographic visualization of the deposition of a phosphoprotein at the mineralization front in the dentin of the rat incisor. J Cell Biol 1973;56:838–845. [PubMed: 4687917]

71. Zheng L, Hilton JF, Habelitz S, Marshall SJ, Marshall GW. Dentin caries activity status related to hardness and elasticity. Eur J Oral Sci 2003;111:243–252. [PubMed: 12786956]

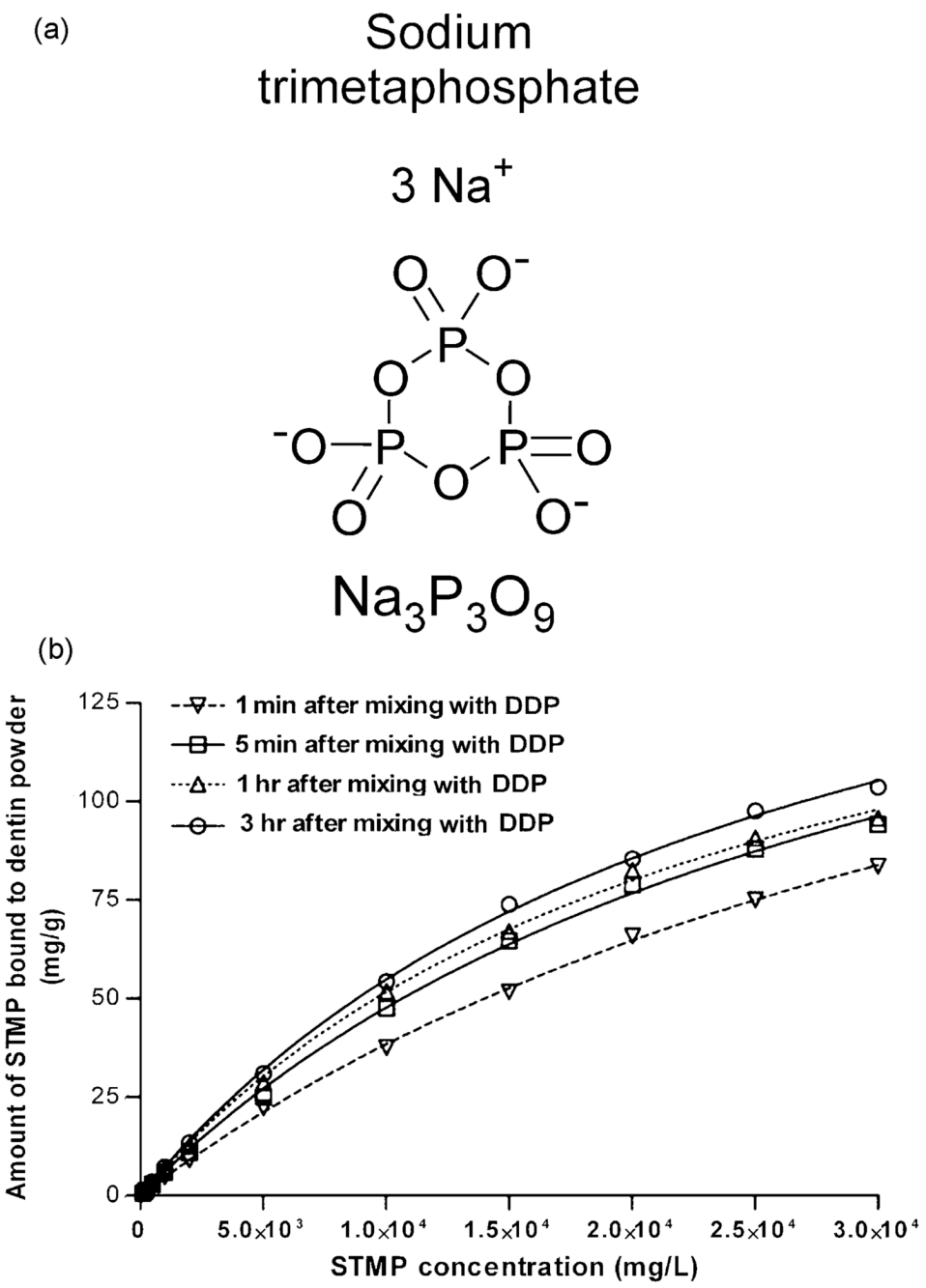

Fig.1.

a. Chemical structure of sodium trimetaphosphate. **b.** Adsorption isotherms produced by the binding of sodium trimetaphosphate (STMP) to demineralized dentin powder (DDP) at 1 min, 5 min, 1 hr and 3 hr at 37 °C, and the corresponding non-linear curve fitting of the experimental data.

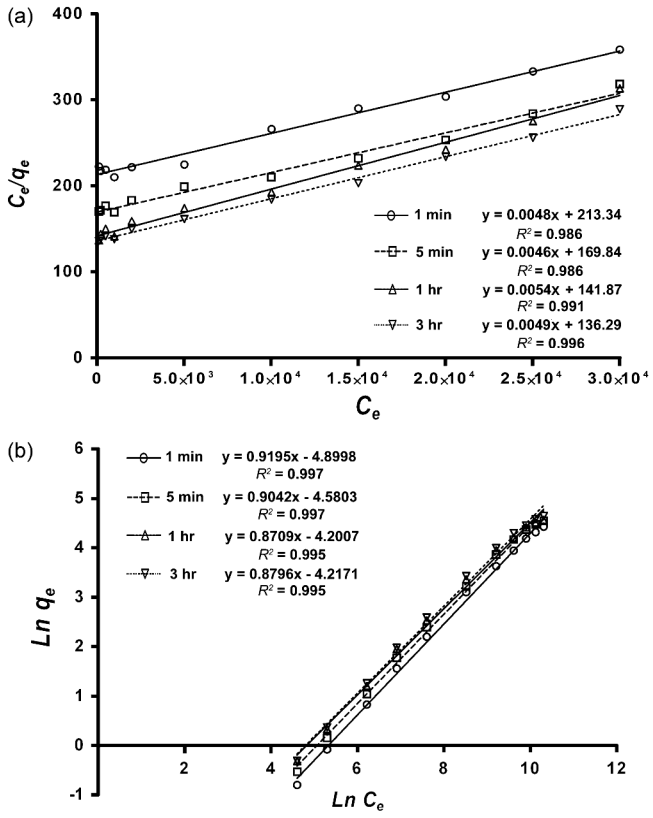

Fig.2.

The Langmuir (a) and Freundlich (b) plots of data in adsorption isotherms of sodium trimetaphosphate (STMP) onto demineralized dentin powder (DDP).

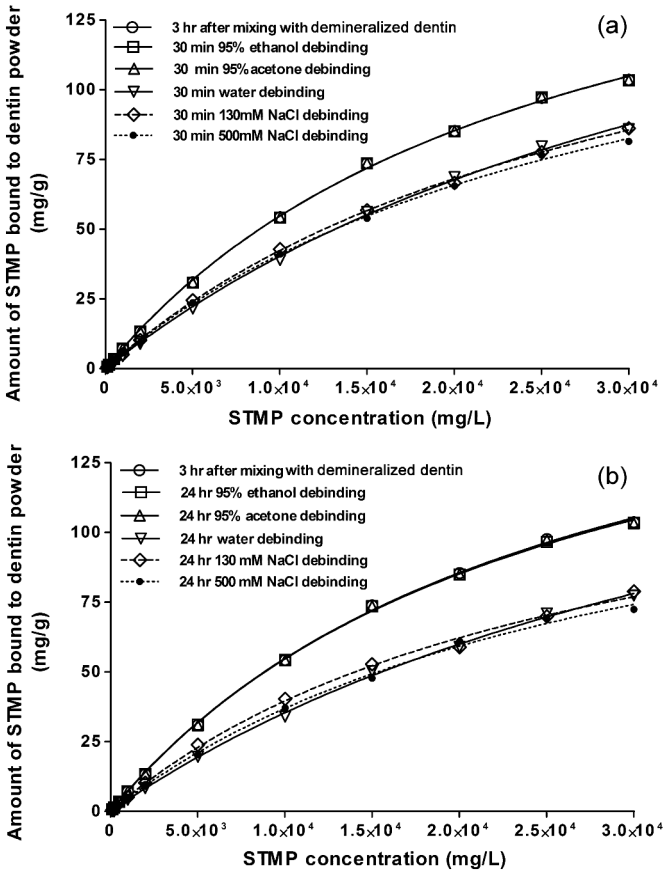

Fig.3.

Desorption isotherms of STMP from STMP-sorbed demineralized dentin powder (DDP) in the presence of organic media (95% ethanol, 95% acetone), and at different NaCl concentrations (0 M, 0.13M, and 0.5 M) at 37°C. The NaCl serves as an ionic species for competitive electrostatic binding. **a.** 30 min; **b.** 24 hours.

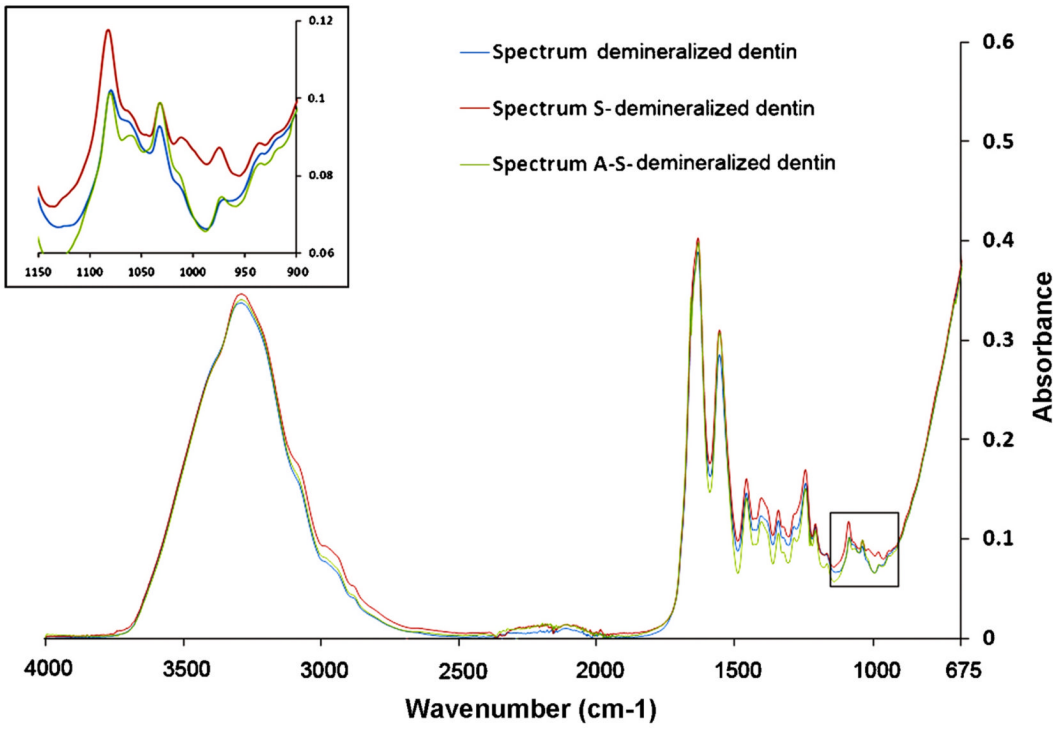

Fig.4.
FT-IR spectra of demineralized dentin powder (spectrum DDP), followed by chemical phosphorylation with 2.5% sodium trimetaphosphate (spectrum S-DDP) and dephosphorylation with alkaline phosphatase (spectrum A-S-DDP).

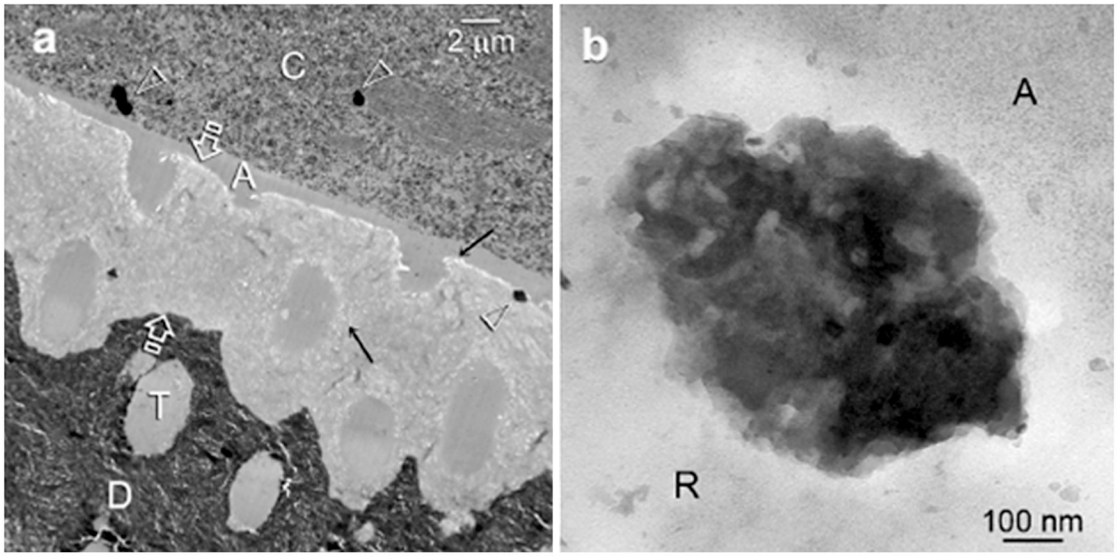

Fig.5.

a. Representative TEM images taken from 4-month sodium trimetaphosphate pre-treated control specimen. No remineralization could be identified within the 5 μm thick zone of resin-infiltrated demineralized dentin (between open arrows). Only 0.3-0.5 μm diameter electron-dense clusters (open arrowheads) were seen within the resin composite layer (C) adjacent to the unfilled dentin adhesive (A), and along the dentin surface. The latter probably represent mineral deposits that were formed within voids in the composite filling (open arrowhead), and those (arrows) that were formed along the adhesive-dentin interface after aging. T: resin-filled dentinal tubule, a characteristic feature of normal dentin; D: mineralized dentin. **b**. A high magnification view of the electron-dense mineral cluster that was found between the dentin adhesive (A) and the resin-infiltrated demineralized dentin (R).

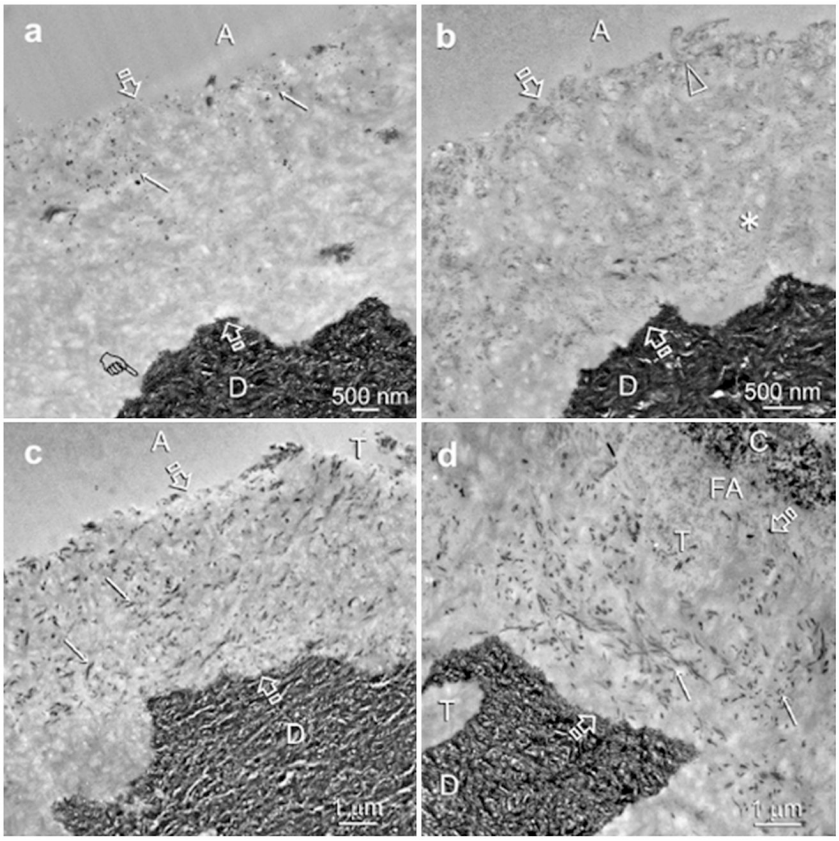

Fig.6.

Unstained, low magnification TEM images taken from different sodium trimetaphosphate pre-treated experimental specimens showing the sequence of events that led to the intrafibrillar remineralization of the incompletely resin-infiltrated demineralized dentin zone (between open arrows) during the 4-month immersion in polyacrylic acid-supplemented remineralization media. Figures a-c were bonded with unfilled One-Step adhesive (A) and fig. d was bonded using the filled XP Bond adhesive (FA). Similar remineralization results were seen for both adhesives. High magnification views of these experimental specimens are illustrated in Figs. 7 and 8. **a**. An early stage of the bottom-up remineralization process in which electron-dense globular phases (arrows) were seen in the resin-infiltrated demineralized dentin. A definitive demineralization front (pointer) was created by the phosphoric acid etchant that was employed to create micromechanical retention for dentin bonding. **b**. An intermediate stage of the bottom-up remineralization process in which very fine electron-dense strands could be identified within the collagen fibrils on the dentin surface (open arrowhead) and the interior (asterisk) of the resin-infiltrated demineralized dentin. **c.** An advanced stage of the bottom-up remineralization process in which electron-dense collagen fibrils (i.e. intrafibrillar remineralization) could be observed within the zone of resin-infiltrated demineralized dentin (arrows). **d**. An advanced stage of remineralization observed in a specimen bonded with the filled adhesive (FA) with a similar manifestation of intrafibrillar remineralization of the collagen fibrils (arrows). C: resin composite; T: dentinal tubules.

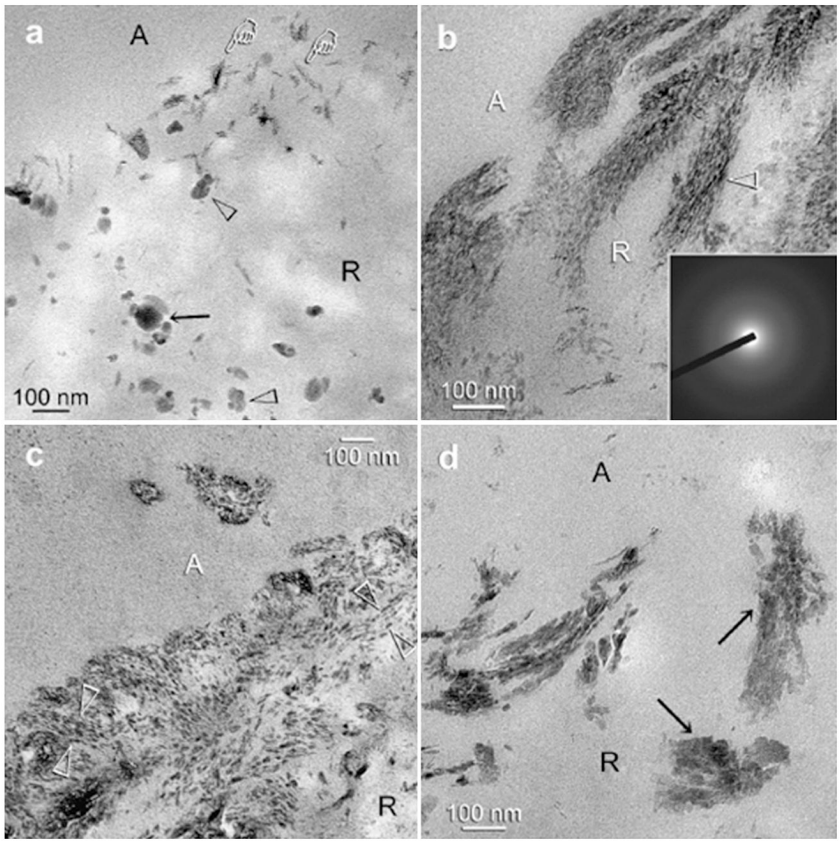

Fig.7.

Unstained, high magnification TEM images of the experimental specimens showing the sequence of events in the remineralization process. The junction between the adhesive (A) and the surface of the resin-infiltrated demineralized dentin (R) is depicted. **a**. An early stage of remineralization corresponding to the low magnification image depicted in Fig. 6a. The larger electron-dense globular phases (black arrow) appeared to be formed by the coalescence of smaller electron-dense globular phases (open arrowhead). They probably represent fluid amorphous calcium phosphate nanoprecursors droplets that had permeated the porous hydrophilic resin matrix. Fine electron-dense microfibrillar strands, not yet fully attaining the dimensions of the collagen fibrils (pointers) could be seen along the surface of the resin-infiltrated demineralized dentin. **b**. Another early stage of remineralization showing the electron-dense, braided microfibrillar strands within the 80-100 nm diameter collagen fibrils (open arrowheads). Selected area electron diffraction (inset) of these microfibrillar strands indicated that the minerals were in an amorphous form at this stage. They probably represent the original water-filled, non-resin-infiltrated spaces within the collagen fibrils that were filled with solidified, coalesced amorphous calcium phosphate as the fluid droplets (Fig. 7a) permeated those microfibrillar spaces. **c**. An intermediate stage of the bottom-up remineralization process corresponding to the low magnification image depicted in Fig. 6b. The continuous, braided, electron-dense microfibrillar strands observed in Fig. 7b had segregated into individual non-overlapping nanocrystals within the collagen fibrils (between open arrowheads). **d**. An advanced stage of the biomimetic process in which large, probably overlapping intrafibrillar platelets could be identified within the collagen fibrils (arrows). Interfibrillar remineralization was minimal as the spaces between the collagen fibrils were filled with the dentin adhesive.

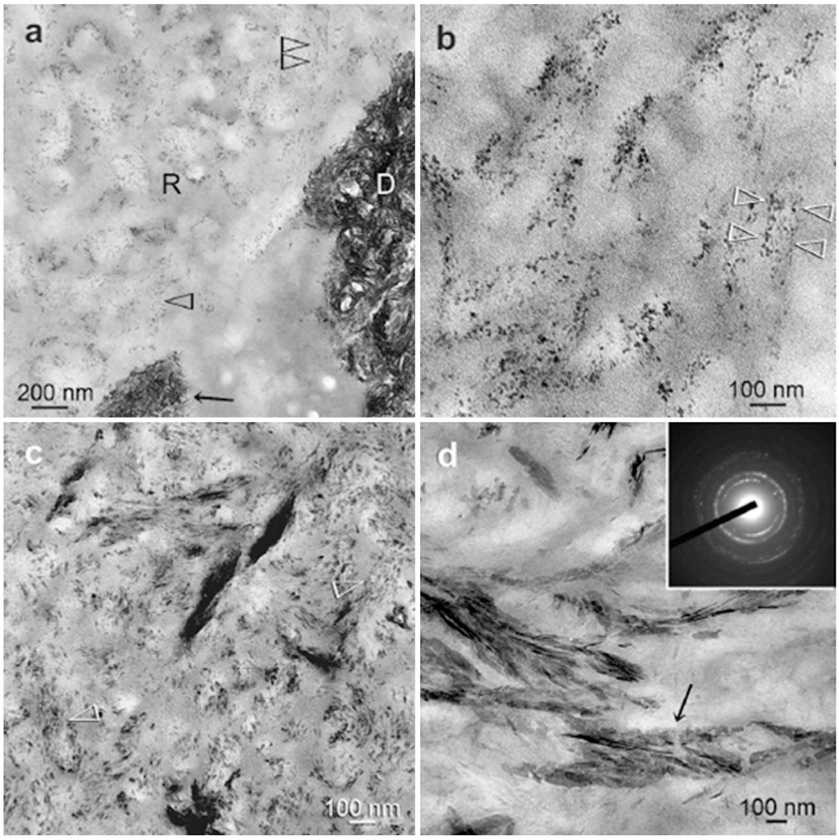

Fig.8.

Unstained, high magnification TEM images of the experimental specimens showing the sequence of events in the remineralization process within the interior of resin-infiltrated demineralized dentin (R). **a**. An intermediate stage of remineralization corresponding to the low magnification image depicted in Fig. 6b in which the collagen fibrils were filled with electron-dense nanocrystals (open arrowheads). These nanocrystals were much smaller in dimensions than those present in the natural mineralized dentin (D). **b**. A higher magnification view of those intrafibrillar nanocrystals within a 70 nm diameter collagen fibril (between open arrowheads). **c.** An intermediate stage of the bottom-up biomineralization process in which non-overlapping intrafibrillar platelets, larger than those depicted in Fig. 8b, were found within the collagen fibrils (open arrowheads) along the orientation of the pleated microfibrils. **d**. An advanced stage of the remineralization process in which overlapping crystallite platelets could be seen within the collagen fibrils (arrow). Selected area electron diffraction (inset) of those crystallites revealed lattice spacings that were characteristic of apatite.

Table I

Summary of isothermal constants and the coefficients of determination (R^2) based on the Langmuir and Freundlich adsorption models

Contact time	Langmuir			Freundlich		
	K_L	q_0	R^2	K_F	n_F	R^2
1 min	2.25×10^{-5}	208.33	0.986	0.0074	1.0875	0.997
5 min	2.71×10^{-5}	217.39	0.986	0.0103	1.1060	0.997
1 hr	3.81×10^{-5}	185.19	0.991	0.0150	1.1482	0.995
3 hr	3.60×10^{-5}	204.08	0.996	0.0147	1.1369	0.995

Table II

Curve fitting parameters from the experimental STMP sorption data based on the one-site specific binding model*

Contact time	1 min	5 min	1 hr	3 hr
B_{max}	206.40 (8.40)	195.90 (9.76)	177.90 (7.28)	194.70 (5.70)
K_d	43791 (2661)	31042 (2582)	24482 (1825)	25483 (1338)
R^2	0.9996	0.9989	0.9989	0.9995

* The one-site specific binding model is represented by the general equation $Y = B_{max}*X/(K_d + X)$, where B_{max} represents the maximum number of binding sites, and K_d represents the sorbent concentration that binds to half the receptor sites in the sorbate at equilibrium.